Waves, Weather, and Ocean Bottom Microseisms[1]

GARY V. LATHAM AND ALI A. NOWROOZI

Lamont Geological Observatory, Columbia University
Palisades, New York 10964

The latest model of the Lamont Geological Observatory Ocean Bottom Geophysical Station (OBS III), located approximately 200 km WNW of San Francisco at a depth of 3.9 km, has been in operation since May 1966. In addition to long- and short-period seismic data, this station provides data on water current direction and speed, water temperature, long- and short-period pressure variations, and horizontal and vertical accelerations at tidal periods. Twenty-three microseismic storms have been detected on the seismic and pressure sensors during the first eight months of operation (May–December 1966). The characteristics of two of these storms have been studied in detail, and the results have been compared with data from the Berkeley seismographs. Both peaks in microseismic activity appear to be related to specific weather systems, one local and one distant. Correlation between local water waves and microseismic amplitudes is observed in one case but not in the other. Particle motion amplitudes on the ocean bottom were 3 to 5 times larger than those at a near-land station (Berkeley) for the vertical component and 7 to 10 times larger for the horizontal component. Predominant periods (6 to 8 sec) were the same at both sites. Ratios of horizontal to vertical particle motion and pressure to vertical motion were measured for microseisms and compared with theoretical values for Rayleigh waves. The combination of these two ratios proves to be a very sensitive method of determining sediment properties. Coherence between pressure and vertical motion is consistently high. It is concluded that (1) the observed microseisms propagate primarily as Rayleigh waves of the fundamental mode, and (2) the thickness of the sediment layer is 0.65 km. The predominant direction of microseismic propagation during both storms was approximately perpendicular to the coastline. Study of the average phase relationship of pressure, vertical particle motion, and horizontal particle motion shows that the direction of propagation is from sea to land if fundamental mode Rayleigh waves are assumed. The microseismic energy flux was approximately 4 times larger in the oceanic structure than in the continental structure near Berkeley for both storms.

INTRODUCTION

Microseisms detected at the ocean bottom by means of the Lamont Geological Observatory Ocean Bottom Geophysical Station (OBS III) are described in this paper. This station is located at 38°9.2'N latitude and 124°54.4'W longitude, approximately 220 km WNW of San Francisco and 220 km south of the Mendocino fracture zone, at a depth of 3.9 km.

The primary elements of the ocean bottom instrument are: (1) a three-component set of pendulums with 15-sec natural periods, (2) a three-component set of pendulums with natural periods of 1 sec, (3) two hydrophones, (4) a vibratron pressure transducer, (5) a water temperature sensor, (6) a current magnitude sensor (Savonius rotor), and (7) a current direction sensor. These instruments (except the pressure, temperature, and current sensors), together with a telemetry system, power convertors, and a command decoder, are housed in three aluminum spheres. Each sphere is 55.9 cm in diameter.

The over-all system orientation after emplacement on the ocean bottom is determined from the current direction sensor. Initially, the direction vane of the current sensor is clamped in a known orientation relative to the instrument frame by a magnesium pin. Until this pin corrodes and releases the vane, about 36 to 48 hours after emplacement, the sensor output gives the orientation of the frame relative to magnetic north. The orientation of the horizontal component seismometers found initially by this method has been verified by phase and amplitude measurements on recorded surface waves. Positive output from the horizontal components H_1 and H_2 corresponds to ground

[1] Lamont Geological Observatory Contribution 1195.

motion along azimuths of 156° and 246°, respectively. These directions are approximately parallel and perpendicular to the local coastline.

Data are transmitted by cable to the recording station at Point Arena, California. The data channels are sampled sequentially and transmitted as an amplitude modulated 8-kHz carrier (see *Sutton et al.* [1965] for details). The demodulated signal is recorded on magnetic tape, strip chart recorders, and photographic drum recorders. A three-component set of short-period seismometers and a wave recorder are now in operation at the Point Arena recording station (38°54′N latitude, 123°43′W longitude).

Commands and ac power (60 Hz) are sent down the cable to the OBS. Thirty separate commands are used to perform the various functions within the OBS. Such functions include change of gain, calibration, leveling, centering, caging and uncaging of seismometers, reference voltage level changes, and division of the vibrotron frequency. The ac power is converted to the required dc levels within the OBS.

OBS III is located on an apron of sediments called the Delgada Fan, which extends approximately 400 km away from the coastline. Bathymetry in this area has been mapped in detail [*Truchan et al.*, 1967]. The location and orientation of the horizontal components are shown in Figure 1.

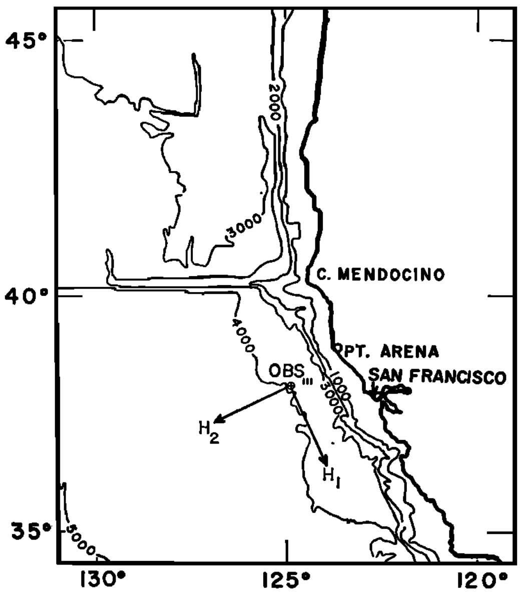

Fig. 1. Location of OBS III. Contour units are meters.

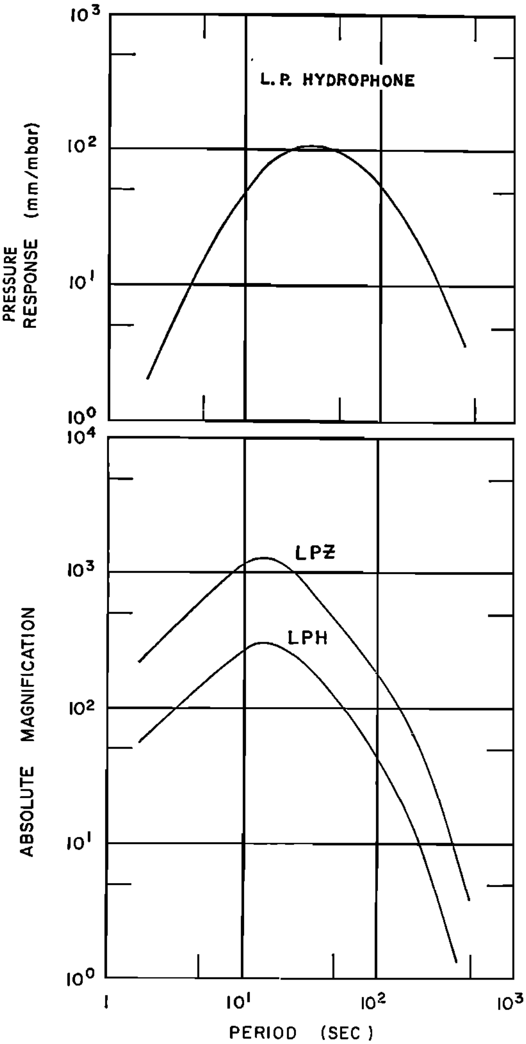

Fig. 2. Response curves for the long-period seismometers and pressure detectors contained in the Lamont ocean bottom geophysical station (OBS III). The ordinate values apply for a recording sensitivity of 4 cm/volt. LPZ indicates the long-period vertical-component seismometer; LPH, the long-period horizontal-component seismometer; L.P. hydrophone, the long-period pressure detector (crystal hydrophone).

The first successful lowering of this instrument system (OBS II) occurred in April 1965. Some results from the OBS II measurements have been discussed by *Sutton et al.* [1965] and *Nowroozi et al.* [1966]. The successful lowering of OBS III was achieved in May 1966. As of this writing, recording has continued for 8 months with no sign of system degradation. In this paper we shall be concerned with data from the seismic and pressure detectors. Response curves for these instruments are shown in Figure 2. Measurements from the current meter, current direction sensor, and vibrotron have been discussed elsewhere [*Nowroozi et al.*, 1968]. Twenty-three clear microseism storms have been recorded during the first 8 months of operation. The characteristics of two of these storms, which have been studied in detail, are discussed in this paper.

General Description of Microseisms

A typical sample of microseisms recorded by the OBS during the second microseism storm, which lasted from June 6 to June 13, 1966, is shown in Figure 3. Note that the crystal hydrophone trace corresponds to the pressure variations at the ocean bottom associated with the propagation of the observed microseisms. Several points are immediately apparent from Figure 3: (1) the amplitudes are larger than those of normal land recordings; (2) the horizontal amplitudes are considerably larger than the vertical amplitudes; (3) the typical 'beat' or group pattern seen on land station records is also seen on the ocean bottom; (4) the H_2 component of horizontal motion is approximately twice the amplitude of the H_1 component; (5) phase correlation between the vertical component and the horizontal component is low; and (6) phase correlation between the vertical component of group motion and the associated pressure variations is high. The predominant period of microseisms in this sample is 7 sec. The relatively large H_2 motion indicates that the direction of propagation is approximately perpendicular to the coastline if the particle motion is longitudinal.

Microseismic amplitudes and periods were measured every 2 hours on the vertical component seismograms from OBS III and Berkeley (BRK) for both microseism storms. In measuring amplitudes, an attempt was made to estimate the peak-to-peak level not exceeded more than 10% of the time. These measurements are plotted in Figures 4 and 5. The corresponding ocean wave amplitudes and periods, as determined by visual observations from the Point Arena lighthouse, are also shown in these figures. Wave measurements are made from the lighthouse every 2 hours unless prevented by poor visibility. The much larger amplitudes for microseisms at the ocean

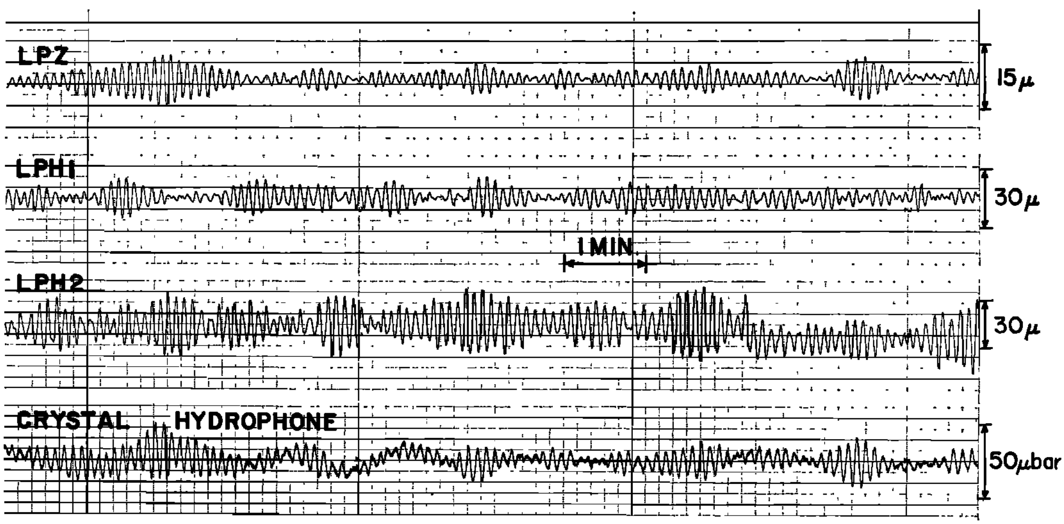

Fig. 3. Sample of microseisms detected on the ocean bottom during the peak of microseism storm 2. The predominant period is 7 sec. LPZ indicates the long-period vertical-component seismometer; LPH, the long-period horizontal-component seismometer.

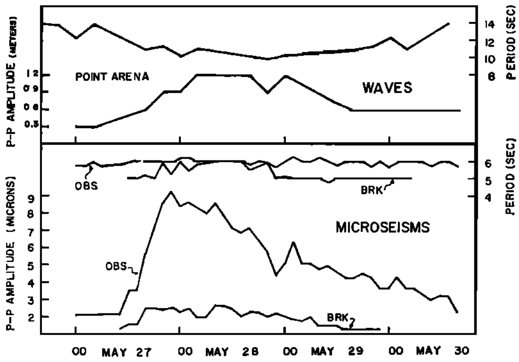

Fig. 4. (*Top*) Ocean wave amplitudes and periods recorded visually during microseism storm 1. (*Bottom*) Amplitudes and periods of microseisms recorded at OBS III and at Berkeley during microseism storm 1.

bottom site as compared with the amplitudes at Berkeley are immediately obvious. The predominant periods are, however, very nearly the same at the two sites during the major part of both storms. Variations in amplitudes with time are also similar, although much less pronounced at Berkeley. It is clear that microseisms measured on the ocean bottom at the OBS site and microseisms measured at Berkeley are closely related. Amplitudes for the first storm (Figure 4) increase very rapidly to a peak within about 12 hours after the first perceptible increase and then decay more slowly over a period of 3 days. The predominant period is about 6 sec at the peak of the storm. Ocean wave amplitudes show a similar variation. Also, the wave periods are approximately twice the microseism periods. The amplitude correspondence and approximate 2-to-1 period ratio support the *Longuet-Higgins* [1950] mechanism for microseism generation.

A similar increase in ocean wave amplitudes is not apparent for the second storm (Figure 5), although the wave periods are again approximately twice the microseism periods. It must be remembered that visual wave measurements are limited to the predominant spectral components. Long-period swell can easily be lost in the shorter-period waves of higher amplitude. The second storm shows a much more gradual increase and decay in amplitudes and a longer duration than the first storm, which suggests a more distant source for the second storm.

Weather maps supplied by the U. S. Weather Bureau, San Francisco, were studied to determine whether the peaks in microseismic activity could be correlated with weather systems. Throughout the period of the first microseism storm, the weather map was dominated by a high-pressure system that moved slowly eastward along latitude 43°N from approximately 160°W longitude to 142°W longitude. A weak low-pressure center and an associated cold front first appeared in the weather map of May

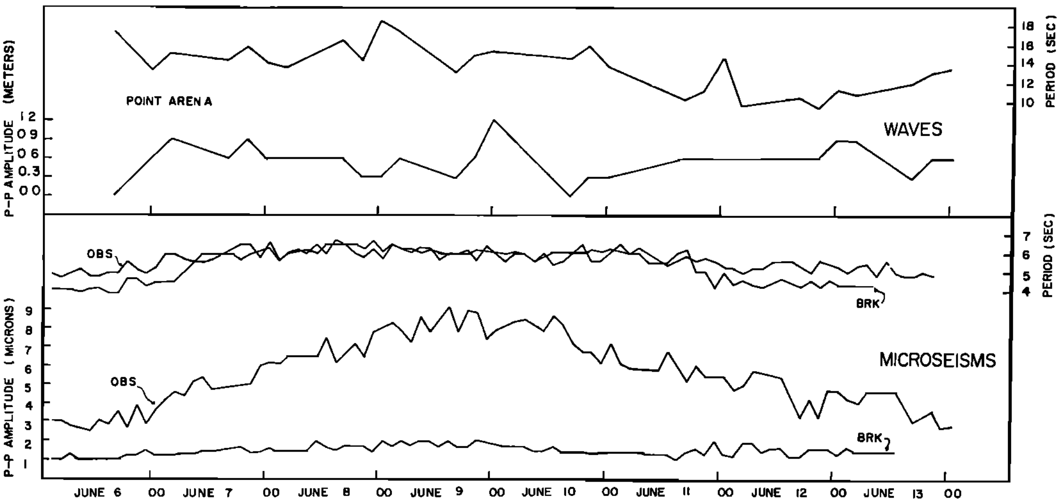

Fig. 5. (*Top*) Ocean wave amplitudes and periods recorded visually during microseism storm 2. (*Bottom*) Amplitudes and periods of microseisms recorded at OBS III and at Berkeley during microseism storm 2.

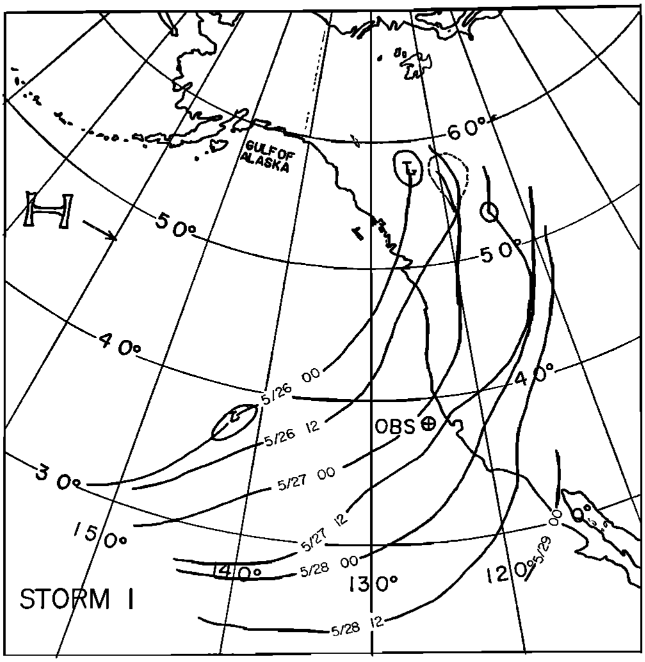

Fig. 6. Weather map showing movement of a cold front over the OBS site during microseism storm 1.

25, 0000 UT; the low was centered in western Canada and the front extended southwest, as shown in Figure 6. The onset of the associated microseism storm occurred at about 1000 UT, May 27. The front at this time was almost directly over the OBS location. Peak amplitudes occurred approximately 17 hours later, when the front had moved several hundred kilometers southeast. The only reasonable conclusion appears to be that this weather system produced the observed microseisms.

The fact that increased microseismic amplitudes were not observed until the wake of the frontal system was directly over the OBS is of considerable interest. Some generation of microseisms must have taken place as the front approached the OBS site and should have been recorded in advance of the actual arrival of the front at the OBS. These results can be explained by assuming that the propagation of microseisms is highly damped in an oceanic structure that includes an appreciable thickness of unconsolidated sediments. This assumption is not unlikely, since an appreciable fraction of the propagating energy at periods of 6 to 7 sec is confined to the sediments that have very low rigidity. This suggestion is further strengthened by the results of studies by *Donn* [1957] and *Latham and Sutton* [1966], which show that microseismic amplitudes at Bermuda and along the east coast of the United States can vary quite independently. This lack of correlation can be explained by assuming that the propagation of microseisms across the ocean basin between Bermuda and the eastern seaboard is highly attenuated.

The weather maps during the second microseisms storm were dominated by a large low-pressure center that reached its maximum development at 0000 UT, June 8, and then gradually diminished as it moved into the Gulf of Alaska. The weather map for this time interval is shown in Figure 7. The track superimposed on the map represents movement of the pressure minimum. Peak microseismic amplitudes were recorded at the OBS at 1800 UT, June 9. Ocean waves arriving at the OBS site at this time would have left the region of maximum cyclonic winds approximately 60 hours earlier, at 0600 UT on June 7. The storm center remained nearly stationary on June 7 while it built up to its maximum intensity. Hence, this storm is a plausible

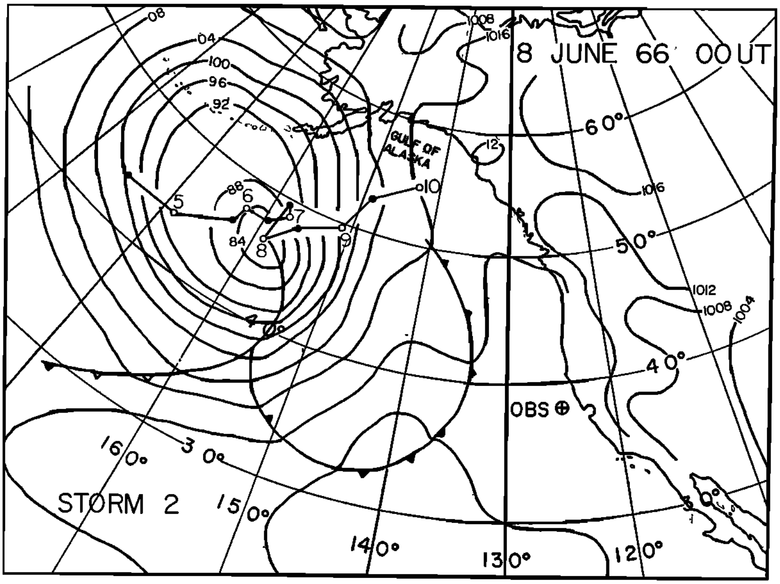

Fig. 7. Weather map showing movement of an intense low-pressure system during microseism storm 2.

source (the only obvious source) for the second microseism storm.

It might be argued that the microseisms of the second storm were generated by wave action along the shore of the Gulf of Alaska and had traversed to Berkeley and the OBS through the continental block. No corresponding peak in activity is observed at College, Alaska, however. It will also be shown in a later section that the direction of propagation is perpendicular to the coastline and from sea to land. If the source were in the Gulf of Alaska, the expected direction of propagation would have been perpendicular to the observed direction. In addition, the gradual increase and decrease in microseismic activity and its long duration suggest a distant source. We conclude, therefore, that wave action in the vicinity of the OBS is the most likely mechanism for generation of the observed microseisms and that the large Pacific low-pressure system is the most likely source for these waves.

Seismograms from the long-period horizontal components show background noise in the period range of 100 to 200 sec. In general, the component that has its sensitive axis parallel to the coast (LPH_1, azimuth 156°) shows larger background noise than the component perpendicular to the coast (LPH_2, azimuth 246°). This ultra-long-period noise appears to be correlated with water current amplitude; i.e., the intervals of highest current speed are correlated with noise level maxima. This noise component appears to be produced by the rocking motion of the entire instrument framework on the soft sedimentary sea floor. Under this hypothesis, the observed motions would be produced by turbulence around the structure. To explain the fact that the motions are larger on one horizontal component (H_1) than on the other, it must be assumed that the motion consists of a rotation about the long axis of the frame. This is the mode of vibration that would be most easily excited in the present case.

Statistical Properties of Microseisms

Power spectral density functions and cross power spectral density functions have been computed for 11.7-min samples of data from the long-period vertical seismometer and the crystal hydrophone. The results are summarized in Figure 8. The two samples shown were recorded during the peaks of the two microseism storms under study. The spectra have approximately 23° of freedom and were smoothed by hamming. Note that the power spectra are in arbitrary units and have not been corrected for instrumental response. The main spectral peaks occur at 6.3 sec for storm 1 and at 7.0 sec for storm 2.

The coherence between pressure P and vertical particle motion Z is close to 1 over the bandwidth of the spectral peak but drops off sharply outside this band. The corrected phase angle between pressure and displacement is near 180° in both cases. This value is the expected phase relationship for a Rayleigh wave propagating in an oceanic structure. To avoid the possibility of confusion in instrument polarities, the phase angle between pressure and vertical particle motion was measured on OBS records for surface waves from a nuclear explosion, where it is certain that we are dealing with Rayleigh waves. The surface wave period is approximately 7 sec, i.e., the same as for the observed microseisms. The phase angle for the surface waves is the same as that observed for microseisms. Thus, for the storms studied, we can say that the phase relationship between pressure and vertical particle motion is the same for Rayleigh waves and ocean bottom microseisms of equal period, independent of the various instrumental phase corrections involved.

It should be noted here that peaks in the microseismic spectra having the same period as concurrent ocean waves were not observed for either storm. Several 1-hour samples of data were analyzed in an attempt to resolve possible longer-period peaks. This result is in contrast to the results of *Latham and Sutton* [1966], *Latham et al.* [1967], and *Haubrich et al.* [1963], who found microseismic spectral peaks

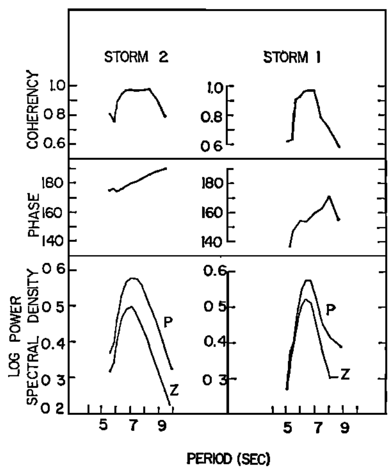

Fig. 8. Coherence and phase between pressure and vertical particle motion and their separate power spectra for both microseism storms.

at periods equal to, and ½ times, the ocean wave period. The absence of the longer-period microseisms in this study may simply be explained by the relatively low amplitudes of the ocean waves.

Coherence between vertical and horizontal particle motion has been computed for times of peak microseismic amplitudes during both storms and has been found to be quite low in all cases: less than 0.2 for Z and H_1 and less than 0.5 for Z and H_2. This is the expected result if, instead of a unidirectional source, microseisms arrive at the detector from many directions with random phases [*Schneider*, 1964; *Strobach*, 1965]. In contrast, coherence between vertical particle motion and pressure is greater than 0.95 in all cases.

Mode of Propagation and Energy Flux of Microseisms

We concluded in the second section that the most likely mechanism for generation of the observed microseisms was water wave interaction in the vicinity of the OBS. It was shown in the preceding section that the measured phase angle between pressure and vertical particle motion was approximately equal to the angle expected for Rayleigh wave propagation. There is abundant evidence from previous studies to support the view that microseisms propagate primarily as Rayleigh waves of the fundamental mode in both oceanic and continental structures [*Latham and Sutton*, 1966]. We will test this hypothesis for the present case in two ways: by comparing the measured ratios of pressure to vertical particle velocity (P/V) and horizontal to vertical particle motion (H/Z) with the theoretical values for both ratios for fundamental and higher mode Rayleigh waves. Three models for the structure at the OBS site, as listed in Table 1, have been assumed. Data for model P-1 based on refraction work at sea were provided by R. W. Raitt (personal communication, 1966).

For the purpose of computation, the sedimentary column has been divided into six layers. The assignment of velocities and densities within these layers is based on the work of *Houtz and Ewing* [1964] and *Nafe and Drake* [1963]. Models P-2 and P-3 are identical with P-1 except for sediment layer thickness. The water layer is taken to be 3.8 km thick rather than

TABLE 1. Layer Parameters for Eastern Pacific Ocean Crustal Models

Layer Thickness, km	Compressional Velocity, km/sec	Shear Velocity, km/sec	Density, g/cc
	Model P-1		
3.800	1.51	0.00	1.03
0.010	1.51	0.15	1.65
0.100	1.60	0.19	1.70
0.100	1.71	0.37	1.79
0.100	1.80	0.53	1.86
0.200	1.90	0.70	1.90
0.500	2.20	1.10	2.05
1.400	4.70	2.70	2.54
4.600	6.90	3.98	2.90
∞	8.20	4.56	3.40
	Model P-2		
3.800	1.51	0.00	1.03
0.010	1.51	0.15	1.65
0.100	1.60	0.19	1.70
0.100	1.71	0.37	1.79
0.100	1.80	0.53	1.86
0.200	1.90	0.70	1.90
0.150	2.20	1.10	2.05
1.400	4.70	2.70	2.54
4.600	6.90	3.98	2.90
∞	8.20	4.56	3.40
	Model P-3		
4.000	1.52	0.00	1.03
0.01	1.52	0.15	1.65
0.10	1.60	0.19	1.70
0.10	1.71	0.37	1.79
0.10	1.80	0.53	1.86
1.30	4.73	2.74	2.50
5.10	6.65	3.74	2.81
∞	8.04	4.60	3.40

the measured thickness of 3.9 km, but the effect of this difference is negligible for the short periods considered here.

The theoretical ratio curves and corresponding experimental points are shown in Figures 9 and 10. In both cases the fit is reasonably close for the fundamental mode and model P-2.

It can be seen from these curves that the P/V ratio is very sensitive to sediment thickness for periods less than 15 sec for the fundamental mode but is insensitive to sediment thickness for the first shear mode. In contrast, the H/Z ratio is more sensitive to sediment thickness for the higher modes than for the fundamental mode. The combination of these two ratios is, thus, complementary in the determination of sedimentary properties from Rayleigh wave propagation.

Note that the theoretical particle motion ratios apply to a single wave train, whereas we are lead to believe, because of the low coherence between H and Z, that microseisms observed at a given point consist of the superposition of waves arriving simultaneously from many directions and with random phases. This superposition of waves would modify the theoretical ratio to some extent [*Strobach*, 1965].

We next consider the energy flux for microseisms in the oceanic structure and the continental structure. The method of computing mean energy flux density used here has been described by *Latham and Sutton* [1966]. For convenience, we have computed the two reference curves that give energy flux density in the two structures as a function of period for a Rayleigh wave of the fundamental mode (Figure 11). The crustal model assumed for the Berkeley region is given in Table 2. The energy flux density at any period corresponds to a constant amplitude of 1 μ (P–P) of vertical motion at a fixed depth. The reference depth is at the free surface for the continental structure and at the top of the sediments for the oceanic structure, i.e., at the point of measurement for both structures. The energy flux density for a Rayleigh wave of the fundamental mode of given period T and vertical particle motion amplitude A (microns) measured at the reference depth is determined from the graph by multiplying the ordinate value corresponding to T by A^2.

At the peak of the first storm, the vertical particle motion on the ocean bottom was 3.5 times larger than at Berkeley. The predominant period was 6.3 sec. Hence, from Figure 11 we see that the energy flux density was 3.6 times larger in the oceanic structure than in the continental structure. The amplitude ratio during the peak of the second storm was 4.4, and the predominant period was 7.0 sec. Hence, the flux ratio for this case is 4.3. In both cases the energy flux density is substantially higher in the oceanic structure. This is the result we would expect to find if microseisms are being generated seaward of the continental-oceanic interface and are propagating onto land. Transmission losses by reflection, refraction, and mode conversion

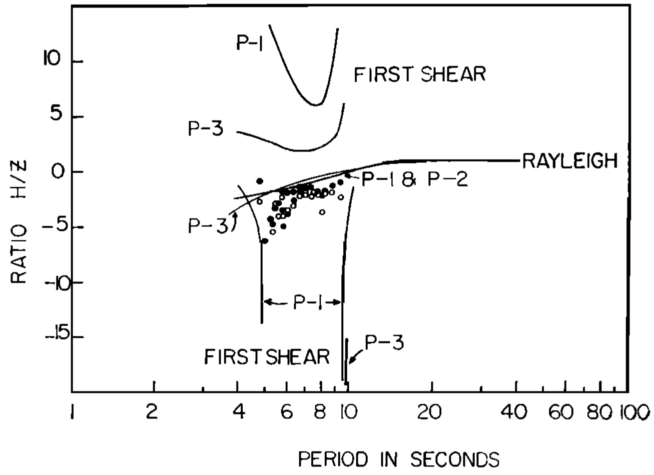

Fig. 9. Theoretical values for the ratio of horizontal to vertical particle motion at the top of the sediment layer (oceanic cases P-1, P-2, P-3) for the first two Rayleigh modes. Experimental points from microseism storm 1 (open circle) and storm 2 (solid dot) are also shown. Positive ratio indicates retrograde motion; negative ratio indicates prograde motion.

of the order measured here are certainly possible.

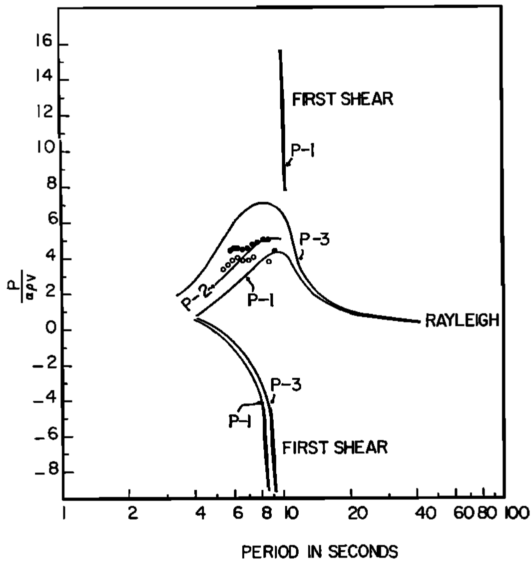

Fig. 10. Theoretical values for the ratio of pressure to vertical particle velocity (P/V) at the top of the sediment layer (oceanic cases P-1, P-2, P-3) for the first two Rayleigh modes. Experimental points for microseism storm 1 (open circle) and storm 2 (solid dot) are also shown. Note that the pressure-to-velocity ratio is divided by water density (ρ) and water sound velocity (α) to make the ordinate scale dimensionless. Positive ratio indicates that P leads V by 90°; negative ratio indicates that P lags V by 90°.

Note that model P-1, with 1 km of sediment, is used for the oceanic structure instead of model P-2, with 0.66 km of sediment, even though P-2 was shown in the above discussion to fit the ratio data better. The energy flux calculations preceded the work that led to the adoption of model P-2. The effect of the thinner sediment layer on the energy flux calculations would

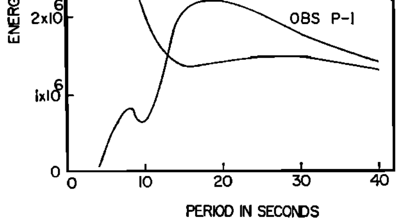

Fig. 11. Energy flux associated with Rayleigh waves of the fundamental mode for the oceanic case (P-1) and the continental case (BRK). The numerical values correspond to a vertical particle motion amplitude (peak to peak) of 1 μ at the top of the sediments in the oceanic case and at the free surface in the continental case.

TABLE 2. Layer Parameters for Berkeley (BRK) Model

Layer Thickness, km	Compressional Velocity, km/sec	Shear Velocity, km/sec	Density, g/cc
5.0	5.60	3.10	2.67
16.0	6.20	3.40	2.80
29.0	7.90	4.39	3.30
∞	8.20	4.56	3.40

be too small, however, to warrant repeating the calculations. The effect would be to increase the oceanic flux relative to the continental flux.

Direction of Propagation of Microseisms

As mentioned above, microseismic amplitudes on the H_2 component are consistently larger than the microseismic amplitude of the H_1 component by a factor of approximately 2. Thus, we can say immediately that the direction of propagation is approximately perpendicular to the coast for both storms if the particle motion is longitudinal.

If the observed microseisms propagate as normal mode waves, the direction of propagation can be determined by measuring the phase relationships between the horizontal and vertical components of motion. For a Rayleigh wave of period $2\pi/\omega$, the horizontal H and vertical Z particle motion at a fixed point can be expressed by

$$H = A \cos \theta \cdot \cos \omega t \tag{1}$$

$$Z = (A/K) \sin \omega t \tag{2}$$

where K is the ratio of horizontal to vertical particle motion amplitude and θ is the angle between the direction of propagation and the sensitive axis of the horizontal seismometer. Written in this form, H leads Z by 90°. For microseisms, however, the observed particle motion results from the superposition of multiple wave trains arriving at the detector from different directions and with random phases. The phase relationships between the horizontal and vertical components of this summed signal may not be consistent on the records. Often the source is sufficiently distant to produce a nearly unidirectional propagation path, and the phase relationships can be determined by direct measurement on the records. If this is not so, as in the present study, the phase relationships must be established on a statistical basis by using a time-averaging process. For the present case, an analog method as described previously by *Latham and Sutton* [1966] was used. Consider the quantity $I = \langle H \times \dot{Z} \rangle$, where the angle brackets indicate the time average of the quantity within the brackets over some specified time interval and $\dot{Z}$ is phase-shifted from Z by 90°. By substituting for H and $\dot{Z}$ from (1) and (2), it is easily shown that I has a finite value for a Rayleigh wave. The sign on I will be plus or minus depending on whether H and $\dot{Z}$ are in phase or 180° out of phase. Hence the integral of I will increase in the plus or minus direction for Rayleigh waves. The quantity I and its integral were formed on an analog computer from magnetic tape playback. Examples of the results are shown in Figure 12. The times of the two samples shown correspond to the peaks of the two microseism storms. Averaging in this case was done with a low-pass filter with a time constant of 40 sec; hence, we have in effect a running average over about six cycles of the signal. The values of the integrals for $\langle H_2 \times \dot{Z} \rangle$ definitely trend toward negative values for both storms, whereas the integrals for $\langle H_1 \times \dot{Z} \rangle$ are near zero in both cases. The polarities are such that negative values indicate propagation in the minus H direction (NE and NW) if the particle motion is prograde and in the plus H direction (SW and SE) for retrograde particle motion. We have presented evidence in the preceding section supporting the view that the observed microseisms propagate primarily as Rayleigh waves of the fundamental mode. Particle motion for the fundamental mode is prograde in the microseismic period range for all models studied to date; hence, the direction of propagation is from sea to land and approximately perpendicular to the coast line for both the local and the distant storms studied. This sea-to-land propagation is in contrast to the case studied near Bermuda [*Latham and Sutton*, 1966], where the direction of propagation was determined to be from the island coastline toward the OBS.

This result indicates that generation of the observed microseisms occurred predominantly seaward of the OBS, i.e., at a distance from shore greater than 200 km. Hence, either ocean wave interaction was more intense in this region than in the region nearer to shore, or the effi-

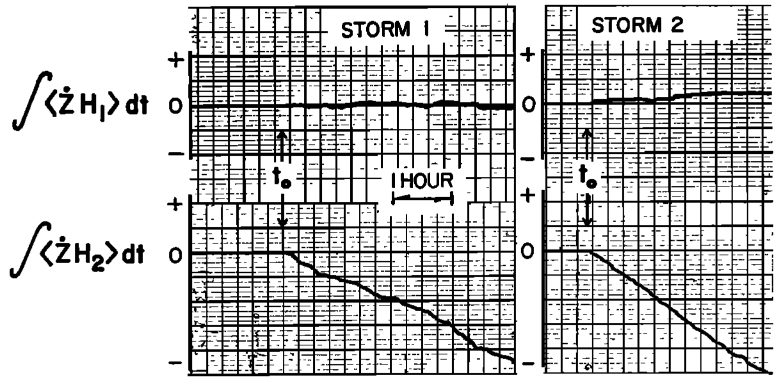

Fig. 12. Integrals of the products of horizontal and vertical particle motion amplitudes recorded during microseism storms 1 and 2. Positive integral values indicate that propagation is in the 'up' or positive direction of the respective horizontal component for prograde particle motion. Negative integral values indicate propagation in the 'down' direction of the given horizontal component. Hence, propagation is approximately in the 'down' H_2 direction for both storms, i.e., from sea toward land and approximately perpendicular to shore.

ciency with which the effective source function couples energy into the water-solid acoustical system is greater in the deeper water. These results do not mean that generation was confined exclusively to the deep-water zone. To the contrary, it was concluded, from the low coherence between horizontal and vertical particle motion, that some microseismic energy arrives at the OBS from all directions. The principal contribution must, however, be from the seaward side of the OBS. The above results are consistent with the results of *Haubrich et al.* [1963], who concluded that the zone of generation, for microseisms recorded at La Jolla, extended outward from the shore line approximately 400 km.

Summary and Conclusions

The major findings resulting from this study are summarized below.

Microseisms recorded on the ocean bottom in deep water off the coast of northern California have nearly the same predominant period and similar amplitude variations as microseisms recorded on land at a coastal site. The amplitudes on the ocean floor are much larger than the amplitudes on land.

Microseismic energy flux is approximately 4 times greater in the oceanic structure than in the continental structure.

The observed microseisms propagate primarily as Rayleigh waves of the fundamental mode for the cases studied. The direction of propagation is from sea to land and is nearly perpendicular to the coastline.

The observed microseisms were produced by two very different types of weather system: (1) a large Pacific cyclone and (2) a local cold front. Wave action in the vicinity of the OBS is the most likely mechanism for generation of the observed microseisms. Wave periods are approximately twice the microseism periods. The Longuet-Higgins mechanism for generation of microseisms is supported by the results of this study. Since the principal contribution to microseismic energy arriving at the OBS during the two storms studied came from the seaward side of the OBS, it must be concluded that generation took place principally in a zone greater than 200 km from shore.

Propagation of microseisms is highly damped in an oceanic structure that includes an appreciable thickness of sediments.

The ratios of pressure to vertical particle motion and horizontal to vertical particle motion are very sensitive and complementary parameters for the determination of sediment properties from short-period Rayleigh waves. Use of this technique yields a sediment depth at the OBS site of approximately 0.65 km.

Acknowledgments. We are indebted to Lee Alsop, Paul Pomeroy, and James Dorman for helpful discussions and for critically reviewing the manuscript. James Dorman kindly gave us permission to use his surface wave program, PV 7, and a second program for computation of the particle motion profiles of Rayleigh waves. The contributions of George Sutton, Stamatios Thanos, William McDonald, and Charles Hubbard in designing and testing the instruments and collecting the data used in this study are gratefully acknowledged. Gordon Hamilton and John Ewing were of great assistance in the emplacement of the instrument system and over-all program management. We gratefully acknowledge the help of B. A. Bolt and the staff of Berkeley Seismographic Station of the University of California.

This research was supported by the Advanced Research Projects Agency under the Vela-Uniform program through the Office of Naval Research (contract NONR 266(92)).

References

Donn, W., A core study bearing on the origin and propagation of 2- to 6-second microseisms, *Trans. Am. Geophys. Union, 38*(3), 354, 1957.

Haubrich, R., W. Munk, and F. Snodgrass, Comparative spectra of microseisms and swell, *Bull. Seismol. Soc. Am., 53,* 27, 1963.

Houtz, R., and J. Ewing, Sedimentary velocities of the western North Atlantic margin, *Bull. Seismol. Soc. Am., 54,* 867, 1964.

Latham, G., R. Anderson, and M. Ewing, Pressure variations produced at the ocean bottom by hurricanes, *J. Geophys. Res., 72*(22), 5693, 1967.

Latham, G., and G. Sutton, Seismic measurements on the ocean floor, 1, Bermuda area, *J. Geophys. Res., 71*(10), 2545, 1966.

Longuet-Higgins, M., A theory of the origin of microseisms, *Phil. Trans. Roy. Soc. London, A,* 243, 1, 1950.

Nafe, J., and C. Drake, Physical properties of marine sediments, in *The Sea,* vol. 3, edited by M. N. Hill, pp. 794–815, John Wiley and Sons, New York, 1963.

Nowroozi, A. A., M. Ewing, J. Nafe, and M. Fliegel, Deep ocean current and its correlation with the ocean tide off the coasts of northern California, *J. Geophys. Res., 73*(6), 1921, 1968.

Nowroozi, A. A., G. H. Sutton, and B. Auld, Oceanic tides recorded on the sea floor, *Ann. Geophys., 22*(3), 512, 1966.

Schneider, W., Ocean-bottom data collection and analysis, *Final Tech. Rept., Contract AF19(604)-8368,* Texas Instruments, Inc., Dallas, Oct. 1964.

Strobach, K., Origin and properties of microseisms from the standpoint of oscillator theory, *Bull. Seismol. Soc. Am., 55,* 365, 1965.

Sutton, G., W. McDonald, D. Prentiss, and S. N. Thanos, Ocean-bottom seismic observatories, *Proc. IEEE, 53,* 1909, 1965.

Truchan, M., C. C. Windisch, and G. R. Hamilton, Detailed bathymetric and seismic reflection survey of a portion of the Delgada deep-sea fan and its channels (abstract), *Trans. Am. Geophys. Union, 48,* 126, 1967.

(Received September 13, 1967;
revised February 9, 1968.)